The EMBO Journal (2010) 29, 2491–2500 | © 2010 European Molecular Biology Organization | All Rights Reserved 0261-4189/10
www.embojournal.org

THE EMBO JOURNAL

The peroxisomal receptor Pex19p forms a helical mPTS recognition domain

Nicole Schueller[1,3], Simon J Holton[1,3], Krisztian Fodor[1], Morlin Milewski[1], Petr Konarev[1], Will A Stanley[1,4], Janina Wolf[2], Ralf Erdmann[2], Wolfgang Schliebs[2], Young-Hwa Song[1] and Matthias Wilmanns[1,*]

[1]EMBL c/o DESY, Notkestrasse 85, Hamburg, Germany and [2]Department of Systems Biology, Faculty of Medicine, Institute for Physiological Chemistry, Ruhr University of Bochum, Bochum, Germany

The protein Pex19p functions as a receptor and chaperone of peroxisomal membrane proteins (PMPs). The crystal structure of the folded C-terminal part of the receptor reveals a globular domain that displays a bundle of three long helices in an antiparallel arrangement. Complementary functional experiments, using a range of truncated Pex19p constructs, show that the structured α-helical domain binds PMP-targeting signal (mPTS) sequences with about 10 μM affinity. Removal of a conserved N-terminal helical segment from the mPTS recognition domain impairs the ability for mPTS binding, indicating that it forms part of the mPTS-binding site. Pex19p variants with mutations in the same sequence segment abolish correct cargo import. Our data indicate a divided N-terminal and C-terminal structural arrangement in Pex19p, which is reminiscent of a similar division in the Pex5p receptor, to allow separation of cargo-targeting signal recognition and additional functions.

The EMBO Journal (2010) **29,** 2491–2500. doi:10.1038/emboj.2010.115; Published online 8 June 2010
Subject Categories: membranes & transport; structural biology
Keywords: biogenesis; peroxisome; receptor; structural biology; translocation

Introduction

Peroxisomes are single-membrane organelles with distinct translocation pathways for peroxisomal matrix proteins and peroxisomal membrane proteins (PMPs). Most matrix proteins include a short peroxisomal-targeting signal (PTS) motif. Two different motifs, categorized as type 1 (PTS1) and type 2 (PTS2), are recognized by the specific receptors, Pex5p and Pex7p, respectively. Structures of the PTS1 receptor Pex5p in the absence and presence of a cargo have unravelled how the conformation of the receptor adapts to recognize peroxisomal matrix proteins through their C-terminal PTS1 motif (Gatto *et al*, 2000; Stanley *et al*, 2006). In contrast, several PMPs have one or more membrane protein-targeting signal (mPTS) motifs with a cluster of basic residues in a predicted α-helical conformation (Fransen *et al*, 2001; Jones *et al*, 2001; Rottensteiner *et al*, 2004). This binding site is generally flanked by one or two transmembrane segments. Correct topogenesis of most of these targets, categorized as class-I mPTS, within the peroxisomal membrane, however, requires two peroxins: Pex3p and Pex19p.

These findings have led to diverse arguments that consider Pex19p as a PMP receptor, an assembly factor, a PMP chaperone or a factor combining more than a single function (Eckert and Erdmann, 2003; Jones *et al*, 2004; Halbach *et al*, 2006). Recent data have reconciled earlier hypotheses by indicating complementary tasks for Pex3p and Pex19p in PMP topogenesis (Pinto *et al*, 2006). In this model, Pexp19p recognizes newly translated PMPs in the cytosol, thus functioning as a soluble PMP receptor. In a second step, the PMP cargo is directed to the peroxisomal membrane by the binding of Pex19p to membrane-bound Pex3p, assigning Pex3p the function of a Pex19p co-receptor (Heiland and Erdmann, 2005; Matsuzono *et al*, 2006; Matsuzaki and Fujiki, 2008). The first step, in which Pex19p shields the hydrophobic PMP Pex19p-binding site, may also be considered as a chaperone-like activity.

Furthermore, there is evidence that Pex19p binds to the docking and assembly complex Pex13p/Pex14p, indicating a functional role in the formation of a multi-component importomer complex (Fransen *et al*, 2004; Neufeld *et al*, 2009). *In vivo*, Pex19p has been found to be associated with the peroxisomal membrane (Gotte *et al*, 1998; Matsuzono *et al*, 1999) and with the ER (Hoepfner *et al*, 2005) showing its dynamic nature and involvement in shuttling processes. The importance of correct peroxisome function is highlighted by the existence of fatal human genetic peroxisomal biogenesis disorders. For example, a frame-shift mutation to the Pex19p coding region (Met255) is one of the underlying causes of Zellweger syndrome (Matsuzono *et al*, 1999).

Pex19p is a soluble 299-residue protein with a conserved C-terminal farnesylation site (Kammerer *et al*, 1997; Matsuzono *et al*, 1999). However, little is known about its structural organization. On the basis of an analysis of splice variants and available binding data, a three-domain organization of Pex19p was proposed (Mayerhofer *et al*, 2002). Limited proteolysis and biophysical data indicated that Pex19p consists of a folded C-terminal part, preceded by a flexible N-terminal sequence (Shibata *et al*, 2004). Mutagenesis data have mapped the primary PMP-binding site to the C-terminal Pex19p domain (Fransen *et al*, 2005). Other *in vitro* data indicate that only full-length Pex19p is capable of PMP binding, thus indicating a contribution from the N-terminal part of Pex19p in PMP recognition

*Corresponding author. EMBL-Hamburg, Notkestrasse 85, Hamburg 22603, Germany. Tel.: +49 40 89902 126, Fax: +49 40 89902 149; E-mail: wilmanns@embl-hamburg.de
[3]These authors contributed equally to this work
[4]Present address: ARC Centre of Excellence in Plant Energy Biology, The University of Western Australia, 35 Stirling Highway, Crawley 6009, Western Australia, Australia

Received: 4 July 2009; accepted: 6 May 2010; published online: 8 June 2010

(Shibata *et al*, 2004). In contrast, the N-terminal part of Pex19p is sufficient to bind both Pex3p, which establishes the Pex3p/Pex19p PMP receptor complex, and the peroxisomal assembly factor Pex14p (Muntau *et al*, 2003; Fransen *et al*, 2004; Jones *et al*, 2004; Shibata *et al*, 2004; Neufeld *et al*, 2009). The importance of the very C-terminus of Pex19p varies for different PMP interactions. A splice variant of human Pex19p, lacking residues 273–299, is able to bind Pex3p and the PMPs ALDP, ALDRP and PMP70 (Mayerhofer *et al*, 2002). To date, there are conflicting reports about the biological impact of Pex19p farnesylation (Vastiau *et al*, 2006). Removing the C-terminal CAAX (A = aliphatic, X = any amino acid) motif, and thus the farnesylation site, from Pex19p, affects its ability to bind several PMPs (Fransen *et al*, 2002; Rucktaschel *et al*, 2009). However, in some investigations, the absence of farnesylation of Pex19p in *Saccharomyces cerevisiae* has no effect on the yeast cell viability (Fransen *et al*, 2001; Vastiau *et al*, 2006).

To unravel the molecular basis of the unusual Pex19p function as both a PMP-docking factor and receptor, we have investigated the natively folded part of Pex19p that comprises the C-terminal segment of the protein sequence. The high-resolution crystal structure of the C-terminal Pex19p domain reveals an α-helical bundle with an overall arrangement that is without precedence in other available protein structures. Quantitative-peptide-binding experiments and complementary functional data show that this domain is a functional mPTS-binding module in Pex19p.

Results

Selection of Pex19p constructs for functional/structural characterization

As a prerequisite for structural analysis of the human Pex19p PMP receptor, we searched for suitable fragments of the protein by combining earlier published data with our own findings. In an earlier investigation, residue 156 was identified as a main proteolytic cleavage site, allowing separation of the N- and C-terminal parts of the protein (Shibata *et al*, 2004). By using a modified proteolysis protocol, we were able to reveal two additional prominent cleavage sites at residue positions 281 and 283 of the Pex19p sequence (Figure 1). On the basis of these data, we selected either residue 283 or the native C-terminus as the protein fragment boundary.

For further functional and structural studies, we used Pex19p constructs with three different N-termini (residues 1, 161, 182). The rational for the choice of residue 161 as the N-terminus was to allow separated structural/functional analysis of the C-terminal part of Pex19p. The full-length version of protein was used as reference for comparison. The third construct with the N-terminus at residue 182 emerged from the structure of the Pex19p C-terminal domain (see below). All three constructs were expressed with two different C-termini (residues 283, 299), generating a total of six different Pex19p fragments for functional characterization (Figure 1A). Folding of all Pex19p constructs investigated was verified by circular dichroism (CD) (Supplementary Figure S1). Whereas the CD spectra of the two Pex19p constructs that include the complete N-terminal part (1–283, 1–299) indicate a significant unfolded protein content, in agreement with earlier biophysical data (Shibata *et al*, 2004), the spectra of all remaining wild-type constructs were basically indistinguishable and indicate that the C-terminal part of Pex19p is mostly α-helical.

C-terminal part of Pex19p folds into an α-helical bundle domain

We were able to crystallize the Pex19p(161–283) fragment (Figure 1A), which includes all conserved Pex19p sequence segments for which an unambiguous multiple sequence alignment is possible (Figure 1B, orange boxes). The X-ray structure of Pex19p(161–283) was determined at a resolution of 2.05 Å, using experimental phases from xenon-derivatized crystals of the protein (Table I). The final model of the structure includes residues 171–280; the remaining residues at the two termini lack interpretable electron density. Mass spectrometry confirmed that there was no further degradation of the crystallized protein (data not shown), indicating that these missing residues adopt flexible conformations within the crystal.

The structure of Pex19p(161–283) reveals that this part of the protein folds into a three-helical bundle domain α2–α3–α4, preceded by a highly exposed N-terminal helix α1 (Figure 2). The overall shape of the helical bundle is cylindrical, with approximate dimensions of 25×25 Å^2 across and 50 Å along the cylindrical axis. The first helix of the bundle (α2) displays a 24° kink at the conserved Pro200, thus effectively generating two helical segments, α2′ (185–197) and α2″ (199–210). The two long 5-turn helices α3 (212–233) and α4 (240–261) form an antiparallel arrangement and pack against helix α2′ with a tilt angle of about 30°. Residues 262–283, constituting the C-terminal region of the Pex19p(161–283) construct, do not adopt any significant secondary structural motifs. In the crystal structure, this sequence segment associates with other parts of the structure in such a way that the hydrophobic core of the three-helical bundle domain is shielded from the solvent environment (Figure 2A).

Overall similarity among Pex19p sequences from different organisms is limited mostly to the helical bundle structure and the preceding helix α1 (Figure 1B, orange boxes), whereas the sequences of the connecting loops and the C-terminal part of the structure substantially differ and cannot be reliably aligned. Most of the conserved and invariant residues of Pex19p(161–283) are either involved in the formation of the Pex19p(161–283) helical bundle core or are surface exposed (Figure 2B, orange).

The first N-terminal helix visible in the structure (α1, 172–183) does not pack against other parts of the structure and is highly exposed (Figure 3). The surface of this helix shows an extensive hydrophobic patch from several conserved amino acids or residues with conserved hydrophobic side chain properties (Figure 3, coloured in green). The side chains of these residues (Ile171, Met175, Ile178, Met179, Leu182, Val187) align with the face of helix α1, which is oriented towards the part of the cylindrical surface of the Pex19p (161–283) helical barrel, comprising the C-terminus of the structure. The only conserved polar residue from this segment (Gln180) is oriented towards the opposite face of helix α1. The nature and the pronounced exposure of this hydrophobic surface patch markedly differ from other surface parts of the structure, thus suggesting a potential function in Pex19p function (see below). A second distinct polar surface patch is formed by several conserved charged

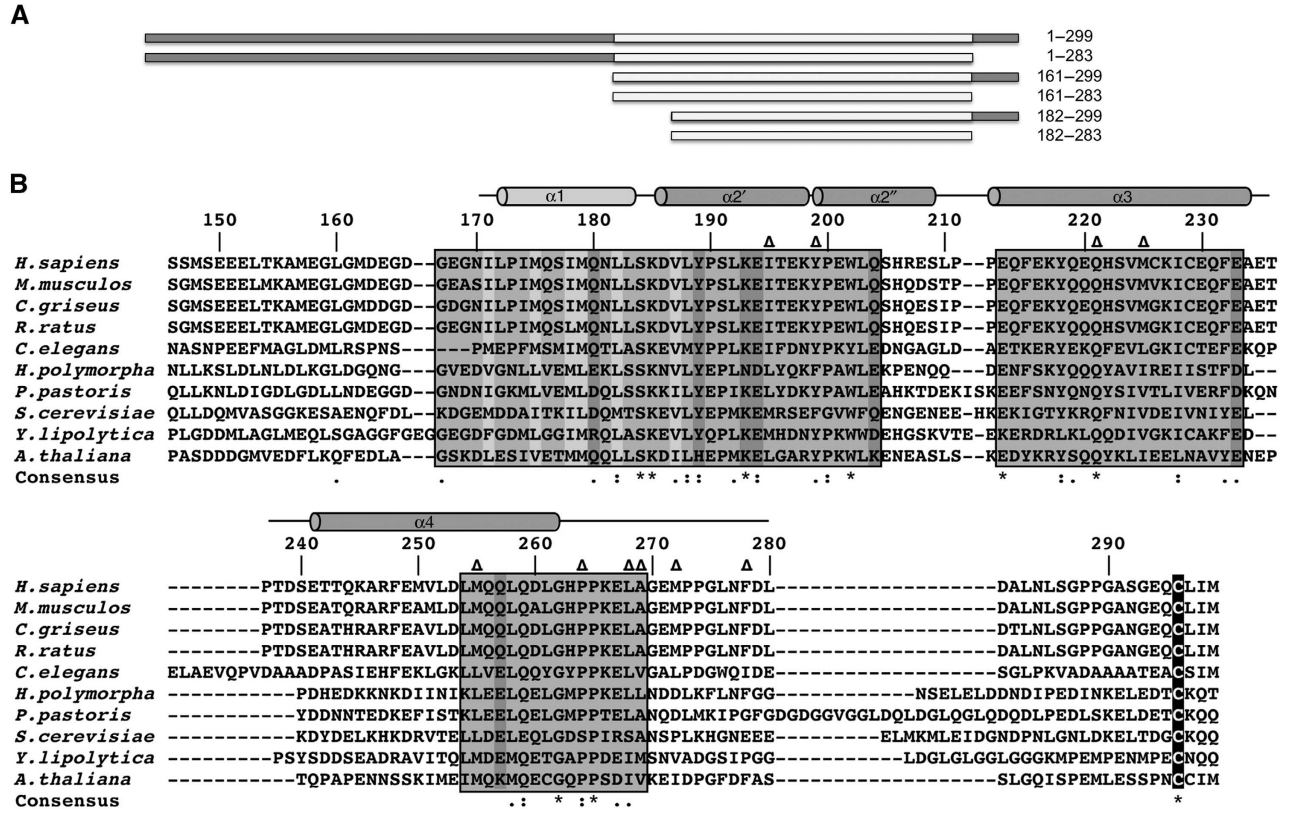

Figure 1 Pex19p sequence/structure relationships. (**A**) Pex19p fragments used for investigation; the sequence segment, whose 3D structure we determined in this study, is highlighted in yellow. The C-termini and N-termini of each protein fragment are listed. (**B**) Multiple sequence alignment of the C-terminal part of Pex19p, showing sequence/structure relationships. A representative set of Pex19p sequences is shown, including *H. sapiens* (UNIPROT code P40855), *M. musculus* (Q8VCI5), *C. griseus* (Q60415), *R. rattus* (Q9QYU1), *C. elegans* (P34453), *H. polymorpha* (Q96WN7), *P. pastoris* (Q9Y8C5), *S. cerevisiae* (Q07418), *Y. lipolytica* (*Q96W74*) and *A. thaliana* (Q9SRQ3). The sequences are quite divergent, thus allowing reliable multiple alignments for restricted sequence segments only (orange boxes). Invariant, highly conserved (maximum one deviating amino acid) and conserved (maximum three deviating amino acids) residue positions are indicated by '*', ':' and '.' symbols, respectively. The sequence numbers refer to the *H. sapiens* Pex19p sequence. The Pex19p sequence segment for which the 3D structure has been determined is indicated by a line above the alignment. Cylinders indicate the positions of α-helices. The mPTS-binding helix α1 is coloured in green. Those residues that are involved in the formation of the central Pex19p cavity (cf. Supplementary Figure S4) are indicated by 'Δ' symbols. Cys296, which presents the C-terminal farnesylation site, is shown in yellow characters and black background. Surface exposed polar amino acids with conserved residue properties are shown on magenta background (cf. Figure 3). Surface exposed hydrophobic amino acids with conserved residue properties are shown on green background (cf. Figure 3). The latter are clustered at the N-terminus of the Pex19p structure, covering helix α1. Sequences were aligned using CLUSTALW (Pearson, 1994), followed by manual adjustments. A full-colour version of this figure is available at *The EMBO Journal* Online.

residues, most of which are located on helix 2α′ (Figure 3, coloured in magenta). One of the residues in this surface patch, Lys193, is invariant (Figures 1 and 2B).

Interestingly, for all four protomers in the asymmetric unit, helix α1 forms an identical antiparallel coiled-coil interaction with the equivalent helix from either a crystallographic or non-crystallographic symmetry-related molecule (Supplementary Figure S2). However, none of our solution data support oligomerization of Pex19p(161–283) or any other Pex19p constructs studied in this contribution (data not shown), suggesting that the observed assembly is transient. Further structural features of Pex19p, including the observation of a large internal cavity, are described in the Supplementary data.

C-terminal helical bundle constitutes the Pex19p mPTS-binding site

In the absence of structural information for Pex19p in complex with PMP target proteins, we became interested in whether the C-terminal domain of Pex19p, as visualized in the X-ray structure, constitutes a functional mPTS-binding element. We, therefore, tested three different Pex19p fragments (1–299, 161–283, 161–299), using an earlier established methodology for PMP-peptide scans (Rottensteiner *et al*, 2004; Halbach *et al*, 2005). The analysis included seven mPTS-peptide motifs from six PMPs, which were scanned in seven two-residue steps each, using earlier published mPTS motifs (Halbach *et al*, 2005) (Figure 4A–D). The remaining four spots of each membrane were used for control experiments. All three Pex19p constructs showed a significant ability for specific binding of most of the selected mPTS peptides. The analysis revealed the strongest binding pattern for peptides from Pex11p, Pex13p, Pex16p, ALDP and the second mPTS motif of Pex26p.

On the basis of these observations and peptide solubility tests, we selected two mPTS peptides, Pex13p and Pex11p, for quantitative binding affinity measurements using fluorescence polarization (FP) (Table II; Supplementary Figure S3). The C-terminal Pex19p(161–283) fragment used for X-ray structural analysis binds the two peptides with equilibrium

dissociation constants of 8.5 and 23.4 μM, respectively. Interestingly, when adding the C-terminal tail (284–299) that comprises the Pex19p farnesylation site, the binding affinity decreases by about five-fold, suggesting a potentially inhibiting effect of the non-farnesylated tail. For comparison, Pex19p versions that include the N-terminal part of the sequence (1–160) show about the same or slightly increased binding affinity as Pex19p(161–283), regardless the presence or absence of the C-terminal tail. The data thus indicate that the C-terminal part of Pex19p is sufficient to recognize the mPTS motif, however, potentially complemented by a presently still uncharacterized, additional function of the N-terminal part of Pex19p in enhancing the mPTS-binding affinity.

We were further interested in identifying the molecular features in the C-terminal helical bundle domain of Pex19p(161–283) that are responsible for mPTS-motif recognition. The high amount of sequence conservation of residues from helix α1 and the presence of an extensive hydrophobic patch generated by the structure of this helix (Figures 1B and 3, coloured in green) suggested that this region of Pex19p could be responsible for mPTS binding. To assess this hypothesis, we expressed and purified two additional versions of Pex19p that lack the corresponding sequence segment (182–283, 182–299). Comparative analysis of the CD spectra of these Pex19p fragments show that their fold content is virtually indistinguishable from other C-terminal Pex19p constructs (Supplementary Figure S1). Initial pepblot analysis revealed that the truncated Pex19p(182–283) construct basically has lost the ability to bind to any of the mPTS peptides used in this qualitative investigation (Figure 4E). Quantitative FP experiments confirmed that for both Pex19p fragments lacking the sequence segment that includes helix α1, Pex19p(182–283) and Pex19p(182–299) have entirely lost the ability to bind to both mPTS peptides (Table II), showing that the presence of helix α1 is essential for mPTS recognition.

In an attempt to further locate residue-specific mPTS-binding sites, we mutated two conserved surface residues from helix α1, Ile178 and Leu182 (Figures 1B and 3), either into a tryptophan or proline, within the Pex19p(161–283) construct that was used for 3D structure determination. The rational of these mutations was to test for potential steric

Table I Crystallographic statistics

	Native	Xenon derivatized
Data collection		
Space group	$P2_12_12_1$	$P2_12_12_1$
Cell dimensions (Å)	$a=67.1$ $b=91.0$ $c=122.3$	$a=67.6$ $b=91.3$ $c=127.7$
Wavelength (Å)	0.98	1.50
Overall resolution range (Å)	73–2.05	55–2.87
Highest resolution range (Å)	2.16–2.05	3.10–2.87
Number of unique reflections	47 467	17 855
Multiplicity	6.2	20.3
Mean $I/\sigma(I)$	7.6 (2.0)	6.2 (2.7)
Completeness (%)	99.6 (100)	99.6 (97.1)
Anomalous completeness (%)	—	99.1 (96.0)
R^a_{sym}	6.2 (45.2)	7.2 (26.2)
Mosaicity (deg)	0.38	0.46
Phasing		
Figure of merit (acentric/centric)	—	0.70/0.62 (0.34/0.29)
Number of sites	—	4
Refinement		
Protein atoms	3717	
Other atoms	192	
R^b_{conv}/R^c_{free}	21.5/25.0	
RMS deviations		
Bond lengths (Å)	0.015	
Bond angles (deg)	1.574	

[a]$R_{\rm sym} = \sum_h \sum_j |I_{h,j} - \langle I_h \rangle| / \sum_h \sum_j I_{h,j}$, where $I_{h,j}$ is the intensity of the jth observation of unique reflection h.
[b]$R_{\rm conv} = \sum_h ||F_{o_h}| - |F_{c_h}|| / \sum_h |F_{o_h}|$, where F_{o_h} and F_{c_h} are the observed and calculated structure factor amplitudes for reflection h.
[c]$R_{\rm free}$ is equivalent to $R_{\rm conv}$, but is calculated using a 5% disjoint set of reflections excluded from the maximum likelihood refinement stages.

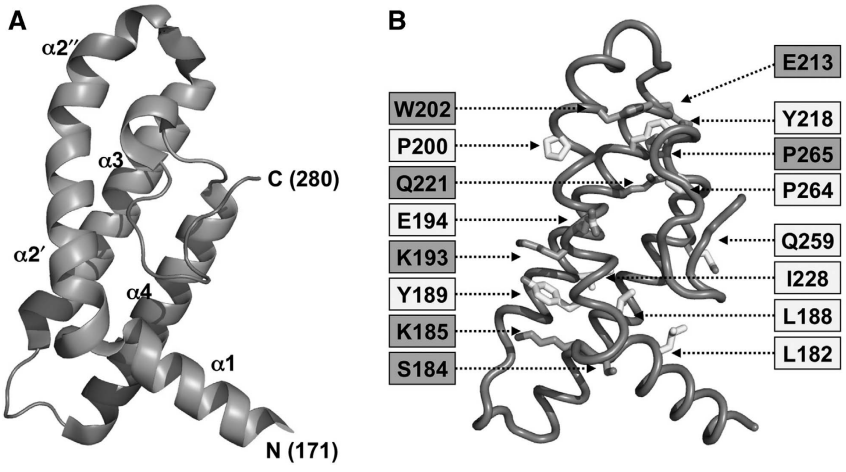

Figure 2 Crystal structure of the mPTS-binding domain of Pex19p(161–283). (**A**) Ribbon representation of the Pex19p(161–283) structure. The secondary structural elements and the termini of the visible part of the Pex19p(161–283) sequence are labelled. Those parts of the structure for which a reliable multiple sequence alignment exists (orange boxes, cf. Figure 1) are shown as orange ribbons. (**B**) Side chains of invariant and highly conserved residues (for definition see Figure 1 caption) of the Pex19p(161–283) structure are shown in orange and yellow, respectively, in stick presentation and are labelled. Oxygen and nitrogen atoms are shown in red and blue, respectively. The illustration reveals that the hydrophobic core of the Pex19p(161–283) helical bundle is most conserved. A full-colour version of this figure is available at *The EMBO Journal* Online.

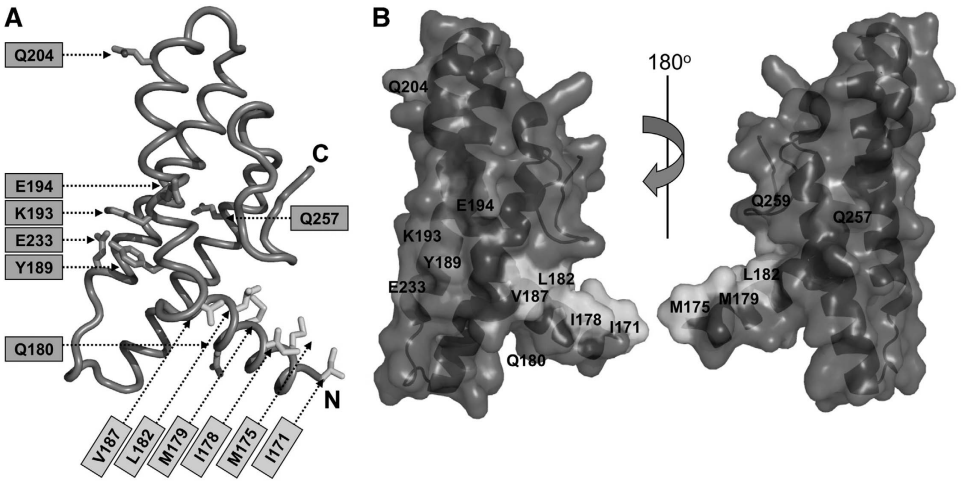

Figure 3 Pex19p(161–283) surface patches with conserved residue properties. (**A**) Worm-type ribbon representation of the Pex19p(161–283) structure; (**B**) semi-transparent surface and ribbon representation of the Pex19p(161–283) structure in two different orientations, in which the right panel is rotated around a vertical axis in the paper plane by 180° with respect to the left panel. The side chain contributions of polar surface residues with conserved amino-acid properties are shown in magenta. The side chain contributions of hydrophobic residues with conserved amino-acid properties are shown in green. All coloured residues are labelled. In the worm-type presentation of the Pex19p(161–283) structure, oxygen, nitrogen and sulphur atoms are shown in atom-specific colours: red, blue, yellow, respectively. A full-colour version of this figure is available at *The EMBO Journal* Online.

clashes and for structural interference of the formation of helix α1. As expected, the Pex19p(161–283, I178P) and Pex19p(161–283, L182P) variants show a slight but significant loss of secondary structural content, most likely because of disruption of helix α1 because of the insertion of a proline residue, whereas the spectra of the two equivalent tryptophan variants were basically indistinguishable with wild-type Pex19p(161–283) (Supplementary Figure S1, panels C and D).

All Pex19p mutants led to a complete or almost complete loss of binding of the Pex11p mPTS peptide, whereas the observed effects on Pex13p binding were not as strong (Table II). Collectively, the data indicate that the binding modes of the two mPTS motifs are probably not identical, which may reflect the lack of specific, directed interactions within a Pex19p-mPTS interface that seems to be dominated by hydrophobic residues from the Pex19p helix α1 (Figure 3) and the two mPTS motifs.

We also tested the importance of helix α1 in Pex19p for mPTS binding *in vivo* by monitoring Pex19p variants for their capacity to functionally complement a peroxisome biogenesis defect in *PEX19*-deficient fibroblasts. Functional complementation restores correct topogenesis of peroxisomal matrix and membrane proteins and formation of peroxisomes. Thus, only those cells in which functional Pex19p enables the correct assembly of peroxin complexes at the peroxisomal membrane exhibit a punctuate pattern for the PTS1-cargo EGFP-SCP, by co-localizing it with the endogenous PMP Pex14p (Figure 5). For this assay, we used the same single-residue Pex19p variants that were investigated for *in vitro* binding of mPTS peptides, however, in context of the full-length Pex19p sequence (Figure 3). In contrast to the tryptophan variants of Pex19p (I178W, L182W), which showed only mild defects, the proline mutants (I178P, L182P) could not rescue the import defect of the Pex19p-deficient cells for EGFP-SCP2 (Figure 5A). After careful inspection of three independent transfection experiments, we could not detect a single cell with a punctuate Pex14p and GFP-SCP2 pattern, although immunolabelling with antibodies directed against Pex19p revealed a transfection rate of up to 50% (data not shown). Western blotting of lysates of the transfected cells revealed similar steady-state levels for all Pex19p variants (Figure 5B). In conclusion, our *in vitro* mPTS-binding data, which characterized both a Pex19p construct lacking the N-terminal helix (182–283) and four additional single-residue mutants, together with complementary *in vivo* functional readout data, which are believed to be sensitive to the complete pool of PMPs needed for peroxisome biogenesis, both identify the same N-terminal region of the C-terminal Pex19p helical bundle domain to be critically involved in mPTS recognition. To what extent the mPTS-binding site is conserved for different PMPs and whether other Pex19p sequence regions are additionally involved, still remain to be determined.

Discussion

Structure of Pex19p(161–283) defines an autonomous mPTS-binding domain

The structural and functional investigation of the C-terminal Pex19p mPTS-binding domain allows us to review earlier findings of the function of Pex19p as a PMP receptor/chaperone (Jones *et al*, 2004). FP analysis with two mPTS peptides from Pex11p and Pex13p shows that the autonomously folded C-terminal Pex19p(161–283) fragment is sufficient to recognize the mPTS motifs from at least two PMP targets (Table II; Supplementary Figure S3), thus allowing its assignment as the Pex19p mPTS-binding domain. These findings are in agreement with a recent study in which penta-peptides were systematically inserted to assess the ability of Pex19p to bind to class-I PMP targets (Fransen *et al*, 2005). All insertion sites that were shown to abolish PMP binding are within the sequence boundaries of the Pex19p(161–283) crystal structure (Supplementary Figure S4). In addition, the loss-of-function insertions are generally located within the α-helices of the structure, whereas most of the insertions with no observed effect are found within the connecting loops.

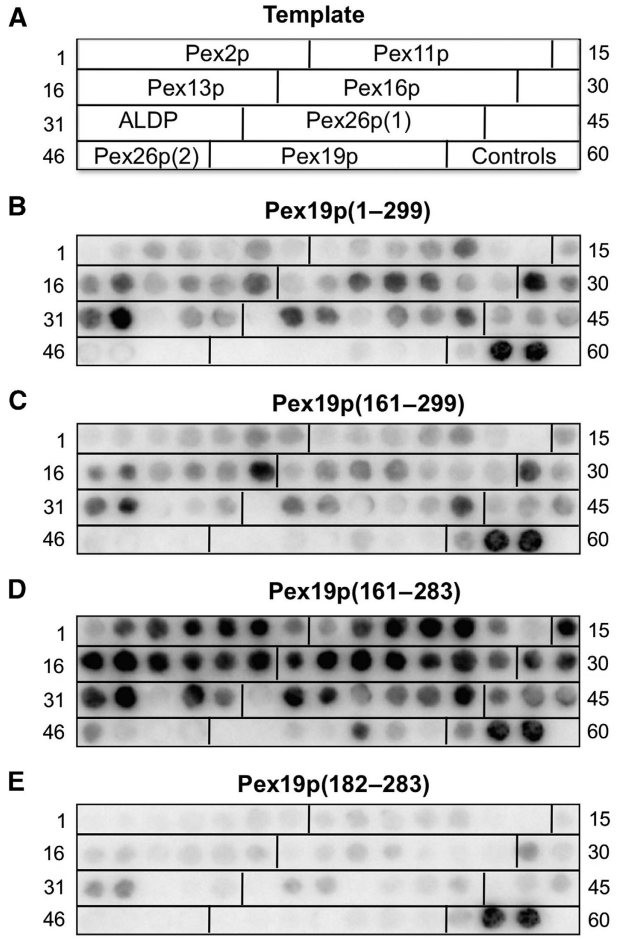

Figure 4 *In vitro* binding of mPTS-peptide motifs by Pex19p. Peptide blot data showing the binding profile of several Pex19p fragments to mPTS peptides. (**A**) Layout of the mPTS motifs (Halbach *et al*, 2005), consisting of 27 residues that were scanned over with 15-mer peptides in two-residue steps, indicated by Pex2p (residues 141–167, FV′IG′LL′KL′GG′LI′NFLIFLQRGKFATLT, spots 1–7), Pex11p-β (residues 180–206, GG′GL′PQ′LA′LK′LR′LQVLLLAR VLRGHPP, spots 8–14), Pex13p (residues 171–197, LK′IH′FT′KV′ FS′AF′ALVRTIRYLYRRLQR, spots 15–21), Pex16p (residues 109–135, RW′LV′IA′LI′QL′AK′AVLRMLLLLWFKAGL, spots 22–28), ALDP (residues 62–88, AA′KA′GM′NR′VF′LQ′RLLWLLRLLFPRVLC, spots 29–35), Pex26p motif-1 (residues 247–273, FF′SL′PF′KK′SL′LA′ALIL CLLVVRFDPAS, spots 36–42), Pex26p motif-2 (residues 270–296, DP′AS′PS′SL′HF′LY′KLAQLFRWIRKAAFS, spots 43–49). In addition, the sequence segment covering helix α1 of Pex19p (residues 164–190, EG′DG′EG′NI′LP′IM′QSIMQNLLSKDVLYP, spots 50–56), the C-terminal PTS1 sequence of mSCP2 (residues 129–143, MKLQNLQLQPGNAKL, spot 57, negative control), a poly-histidine sequence (HHHHHH, spots 58–59, positive control) and an empty spot (60, negative control) were analysed. Spot numbers are indicated to the left and to the right. Experimental data are shown in (**B**) Pex19p(1–299), (**C**) Pex19p(161–299), (**D**) Pex19p(161–283) and (**E**) Pex19p(182–283).

Thus, the data indicate that the structural integrity of the helical bundle found in the Pex19p structure is critical to recognize PMPs (Fransen *et al*, 2005).

A recent study unravelled that, while several Pex19p fragments truncated at residue 261 retain peroxisome-restoring activity, slightly shorter Pex19p constructs, truncated at residue 255, have lost this functional ability (Matsuzono *et al*, 2006). In the structure of the Pex19p mPTS-binding domain, residue 261 coincides with the C-terminus of helix α4 (Figure 2). As the preceding residues (255–260) are involved in the packing of the antiparallel arrangement of the two long helices α3 and α4, the Pex19p truncation data can be interpreted as an indication that the structural integrity of the C-terminal Pex19p domain is critical for its function as an mPTS-binding epitope. The same region is also highly sensitive to structural perturbations (Supplementary Figure S4).

As the first helix α1 points away from the remaining core of the helical bundle in the structure of Pex19p(161–283) and is highly conserved (Figures 1 and 3), we investigated its contribution to mPTS binding separately. A Pex19p(182–283) variant without this helix almost completely abolished the ability to bind several mPTS motifs (Table II), indicating that the corresponding sequence segment in Pex19p is critical for mPTS recognition. These data were corroborated by *in vivo* assays in Pex19-deficient fibroblasts, which confirmed the importance of the helical structure of this sequence segment for maintaining a functional peroxisomal translocation system (Figure 5).

Potential functions of Pex19p sequence segments flanking the C-terminal helical bundle domain

Interestingly, we found a moderate effect in enhancing the overall binding affinity in the presence of the N-terminal part of Pex19p(1–160) (Table II). These data support earlier investigations, which indicated that most of the N-terminal part of Pex19p, which is associated with Pex3p binding and membrane targeting, is required for PMP recognition as well (Shibata *et al*, 2004; Matsuzono *et al*, 2006). These differences could reflect additional functional requirements of Pex19p for PMP recognition, stabilization and import beyond mPTS recognition. These considerations are supported by recent findings that PMP-cargo loading of Pex19p leads to increased binding of the N-terminal part of Pex19p to Pex3p, which is membrane associated and has been characterized as a PMP-docking factor (Pinto *et al*, 2006). Interestingly, there is also increasing evidence for non-mPTS-binding sites in several PMP targets (Vizeacoumar *et al*, 2006), thus raising questions about the exclusiveness of mPTS-binding sites for PMP recognition by Pex19p.

Emerging molecular mechanisms in peroxisomal import receptors

To date, three peroxins have been identified and characterized to function as import receptors: Pex5p, Pex7p and Pex19p. In contrast to the PMP receptor/chaperone Pex19p, Pex5p and Pex7p are receptors for peroxisomal matrix proteins with specific recognition signal sequences (Stanley *et al*, 2007a). Interestingly, the PTS/cargo-binding modules of all three receptors assemble with co-receptor components either by intramolecular interactions with additional domains or by hetero-assemblies with other peroxins (Schliebs and Kunau, 2006), which together allow targeting of the respective receptor/cargo complexes to the peroxisomal membrane.

Notably, Pex5p and Pex19p share the same sequence division, comprising a folded C-terminal PTS-binding domain and a less folded N-terminal segment that is involved in membrane docking of the respective receptor/cargo complexes. Moreover, the two peroxisomal receptors display similar α-helical bundle arrangements. However, whereas considerable conformational changes in the seven-fold repeated TPR array in Pex5p on cargo recognition have

Table II Fluorescence polarization (FP) measurements

Pex19p construct	mPTS(Pex13p)			mPTS(Pex11p)		
	k_D (μM)	R^2 [a]	Relative $1/k_D$	k_D (μM)	R^2 [a]	Relative $1/k_D$
Pex19p(1–299)	8.4 ± 0.9	0.99	1.01	11.8 ± 1.5	0.99	1.98
Pex19p(1–283)	7.2 ± 0.7	0.99	1.18	14.1 ± 1.9	0.99	1.66
Pex19p(161–299)	38.3 ± 5.7	0.99	0.22	85.8 ± 25.4	0.97	0.27
Pex19p(161–283)[b]	8.5 ± 1.4	0.98	1.00	23.4 ± 7.1	0.96	1.00
Structure-based Pex19p mutants						
Pex19p(182–283)	No			No		
Pex19p(182–299)	No			No		
Pex19p(161–283, I178W)	70.1 ± 5.6	0.99	0.12	Weak[c]		
Pex19p(161–283, I178P)	Weak[c]			No		
Pex19p(161–283, L182W)	Weak[c]			No		
Pex19p(161–283, L182P)	31.7 ± 9.0	0.96	0.27	Weak[c]		

[a]Adjusted R^2, expressing the goodness of fit, as defined in Origin version 8 software.
[b]Reference, relative $1/K_D = 1.00$.
[c]Weak binding: $K_D > 100$ μM, quantitative calculation not possible.

been established (Stanley *et al*, 2007b), the type and extent of possible conformational changes on mPTS recognition and PMP recognition by the Pex19p receptor remain elusive to date.

An important distinction of these receptors is associated with different receptor-specific requirements for cargo stabilization. In contrast to Pex19p, for which a parallel chaperone function has been extensively described (Fang *et al*, 2004; Shibata *et al*, 2004), there is no evidence that the other two import receptors, Pex5p and Pex7p, have such an additional function (Schliebs and Kunau, 2006; Stanley *et al*, 2007a). This seems to be plausible in the light that post-translational PMP import requires mechanisms for temporal stabilization of hydrophobic PMP regions. Therefore, it is conceivable to consider additional requirements associated with the N-terminal part of Pex19p and its suggested parallel function as chaperone, as a prerequisite for recognition of most PMPs by Pex19p. Our data suggest that mPTS binding by the C-terminal bundle domain of the Pex19p receptor is sufficient for complete PMP recognition.

Materials and methods

Cloning, expression and protein purification

Escherichia coli strains DH5α and BL21(DE3) were used for plasmid amplification and protein expression, respectively. *Homo sapiens* PEX19 DNA encoding Pex19p(1–299), Pex19p(1–283), Pex19p (161–299), Pex19p(161–283), Pex19p(182–283) and Pex19p(182–299) were cloned into the pETM11 vector, which includes an N-terminal poly-histidine tag with a TEV cleavage site, using the NcoI and BamHI sites. Owing to the presence of an internal NcoI site in the two longest constructs, the 5′ cut was performed with BsmBI to create an NcoI compatible overhang. Single-point mutants were generated with the QuikChange Site-Directed Mutagenesis kit (Stratagene), according to the manufacturer's instructions. All primers that were used to create the different length constructs and the mutants are described in Supplementary Table SI.

BL21 (DE3) cells, transformed with *PEX19* constructs associated with Pex19p(1–299), Pex19p(1–283), Pex19p(161–299), Pex19p (161–283), Pex19p(182–283) and Pex19p(182–299), were expressed in LB medium with protein expression induced by the addition of a final concentration of 0.1 mM IPTG at 20°C for 16 h. Pelleted cells were resuspended in buffer A (100 mM potassium phosphate pH 8.0, 20 mM imidazol and 1 mM β-mercaptoethanol), lysed by sonication, loaded onto NiNTA resin and eluted with buffer B (100 mM potassium phosphate pH 8.0, 500 mM imidazol and 1 mM β-mercaptoethanol). The eluted protein was dialysed overnight into buffer A and simultaneously digested with TEV protease (1:50 molar ratio) to cleave the N-terminal hexa-histidine tag. A second affinity chromatography step removed the protease, affinity tag and undigested protein from the protein of interest, which was concentrated and purified by size-exclusion chromatography. The final proteins were >98% pure as judged by SDS–PAGE (Supplementary Figure S5).

Circular dichroism

CD experiments were performed on a Jasco J-810 spectropolarimeter. Proteins were dialysed into 10 mM potassium phosphate (pH 8.0) and 1 mM DTT. Far UV spectra were recorded between 185 and 260 nm (1 mm cuvette, 0.1 mg/ml protein concentration, as determined by specific absorbance at 280 nm). The machine settings were 1 nm bandwidth, 1 s response, 0.5 nm data pitch and 100 nm/min scan speed. All CD data presented are the averages of three separate experiments.

X-ray structure determination

All expressed and purified Pex19p versions were submitted into crystallization trials at the high-throughput crystallization facility at EMBL Hamburg (Mueller-Dieckmann, 2006). Owing to the high solubility of the constructs, most crystallization drops remained clear or showed phase separation, even using protein concentrations up to 80 mg/ml. Crystal-like structures without sharp edges grew from Pex19p(161–283). After optimization, Pex19p(161–283) at a concentration of 30–40 mg/ml protein in 2.0 M sodium malonate, pH 5.5, yielded single crystals after 2 days at 4°C, suitable for data collection.

The structure of Pex19p(161–283) was solved by the single isomorphous dispersion method from a single crystal. Before X-ray data collection, the crystal was briefly immersed in cryo-protection solution comprising mother liquor supplemented with 30% (v/v) glycerol and subsequently derivatized with xenon for 90 s at 3.5 MPa, using the Hampton Xenon Chamber. After releasing the applied xenon pressure, the crystal was flash frozen in liquid nitrogen. X-ray data were collected on the synchrotron radiation wiggler beamline BW7A at EMBL/DESY, Hamburg, Germany, at a wavelength of 1.5 Å and recorded on a 165 mm MarCCD detector. Data were integrated, scaled and merged using the programs MOSFLM and SCALA (Project, 1994). Manual inspection of the anomalous difference Patterson maps, calculated with the program FFT (Project, 1994), confirmed the successful crystal derivatization by xenon. An additional 2.05 Å resolution dataset was collected from a Pex19p(161–283) crystal, soaked for 5 s in 6 M sodium formate, at a wavelength of 0.972 Å.

The heavy-atom sub-structure was solved using SHELXD through the HKL2MAP graphical user interface (Pape and Schneider, 2004). Four xenon sites were identified from high correlation coefficient values. Using these sites, RESOLVE (Terwilliger, 2003) was subsequently used for density modification, resulting in a readily interpretable electron density map from which an initial model was built using COOT (Emsley and Cowtan, 2004).

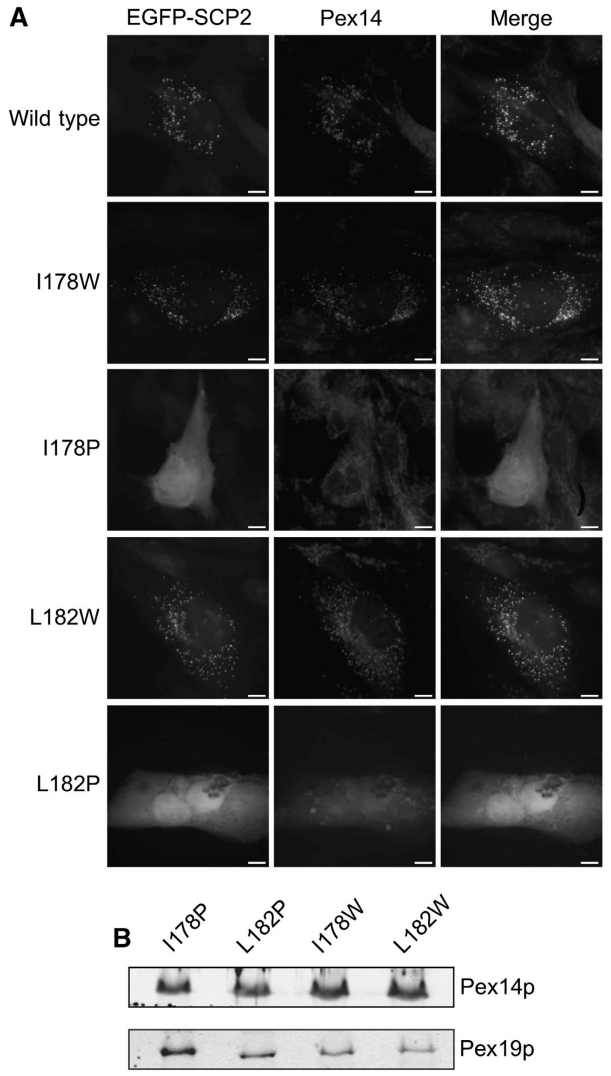

Figure 5 Functional properties of Pex19p variants in *PEX19*-deficient human fibroblasts. (**A**) *PEX19*-deficient fibroblast cells were co-transfected with pEGFP-SCP2 and plasmids expressing either *wt* PEX19 or single-residue mutants as indicated. At 72 h after transfection, cells were analysed for localization of pEGFP-SCP2 by direct fluorescence microscopy (green) and for localization of endogenous Pex14p by immunofluorescence, using antibodies against Pex14p (red). Complementation of the mutant cells by functional Pex19p is indicated by a congruent punctuate fluorescence pattern (yellow), showing the restoration of cargo import and correct formation of peroxisomes. Functional complementation has been observed for Pex19p (wild type), Pex19p(I178W) and Pex19p(L182W). In contrast, no cells with a punctuate pattern were found for transfections with Pex19p(I178P) and Pex19p(L182P). Scale bar, 10 μm. (**B**) Cell lysates, obtained from *PEX19*-deficient cells transfected with expression plasmids encoding Pex19p variants, were analysed by immunoblotting using antibodies directed against Pex14p and Pex19p. A full-colour version of this figure is available at *The EMBO Journal* Online.

Four Pex19p(161–283) protomers could be identified in the asymmetric unit, corresponding to a solvent content of 65%. The initial Pex19p(161–283) model was refined against the high-resolution native dataset through iterative manual rebuilding using COOT and maximum-likelihood refinement with the program REFMAC5 (Project, 1994; Emsley and Cowtan, 2004). TLS-based refinement, with each molecule in the asymmetric unit defined as one TLS group, was also used in the latter stages of model refinement. Ordered solvent molecules were automatically identified with the program ARP (Project, 1994) and manually verified. Statistics for the final model are given in Table I. Coordinates and structure factors have been submitted to the PDB database with the accession code 2WL8.

Peptide blot experiments

Seven 15-mer peptides, scanning earlier characterized mPTS sequence motifs (Halbach *et al*, 2005) with two-amino-acid shifts, were synthesized on a nitrocellulose membrane (provided by C Landgraf, Berlin, Germany). To allow direct comparison of the four different Pex19p constructs used in this study, membranes were designed to comprise four identical arrays of 60 spots (for further details, see caption of Figure 4). Membranes were activated and washed according to published protocols (Rottensteiner *et al*, 2004). All Pex19p constructs used in this study were expressed from the pETM30 vector as His_6-GST fusions and purified as described above. Each membrane was overlayed with 3 ml of 800 nM His_6-GST-tagged Pex19p constructs. Bound protein was detected using a primary monoclonal Anti-His_6 antibody (Novagen), followed by a secondary goat anti-mouse HRP-conjugated antibody (Novagen).

FP-based peptide-binding assays

FP peptide-binding experiments were performed using a FluoroLog-3 spectrofluorometer (HORIBA Jobin Yvon, Germany) (Supplementary Figure S2). The following mPTS peptides, N-terminally labelled with fluorescein isothiocyanate (FITC), were synthesized by Charité (Humboldt University, Berlin, Germany): Pex13p, (FITC)-FTKVFSAFALVRTIR and Pex11p, (FITC)-LALKLRLQVLLLARV. The two peptides were dissolved in methanol at concentrations of 0.1–0.5 mM, before titration against different Pex19p constructs. Owing to the sensitivity of the fluorophore to light, titrations were carried out in a reverse manner, starting with maximum protein concentration, followed by 12 or 13 two-fold dilution steps with buffer containing 0.2 μM FITC peptide. Before each measurement, the solution was equilibrated for 5 min at $20 \pm 0.01^{\circ}C$. The fluorescence signal was recorded at the excitation wavelength of 488 nm and at the emission wavelength of 517 nm. The fluorescence anisotropy (A) signal was determined according to $A = (I_{vv} - G \cdot I_{vh})/(I_{vv} + G \cdot 2 \cdot I_{vh})$, in which the G-factor is defined as the quotient I_{vh}/I_{hh}. The intensities were measured at the four combinations of the excitation and emission polarizers, I_{vh}, I_{hh}, I_{vv} and I_{vh}, respectively. The first subscript stands for the excitation and the second subscript stands for the emission polarizer, respectively (v, vertical and h, horizontal position of polarization plane). The calculated anisotropy values were plotted as function of protein concentration. Using Origin version 8 software (http://www.originlab.com), the titration curves were fitted using the Levenberg–Marquardt non-linear fit algorithm, which is implemented into the software and assumes a binding model of $A + B = AB$. The fit function was that of a modified Hill analysis and has the formula: $y = \mathrm{START} + (\mathrm{END} - \mathrm{START}) \times x^n/(K_d^n + x^n)$, where y is the calculated anisotropy, x is the titrated Pex19p protein concentration and n is the Hill coefficient (Pogenberg *et al*, 2005). For the chosen binding model, the value of n was fixed to 1. The goodness of fit is given with adjusted R^2, which is a validation function in the fitting algorithm of ORIGIN software and should be close to the value 1.

In vivo peroxisome import assays

Point mutations were introduced into the Pex19p expression vector pcDNA3-PEX19 using the Quickchange XL—Site-Directed Mutagenesis kit (Stratagene). All primers used are listed in Supplementary Table SI. Patient-derived *PEX19*-deficient skin fibroblasts (primary cell line *RW/mf/0854872*, kindly donated by R Wanders, AMC, Amsterdam, The Netherlands) were immortalized by transfecting with SV-40 large T antigen. The resulting cell-line ΔPEX19 T was double transfected with one of the plasmids expressing Pex19p (1–299) variants together with pEGFP-SCP2, using the Nucleofector-kit (Amaxa). Human fibroblast cells were cultured as described earlier (Stanley *et al*, 2006). Seventy-two hours after transfection, cells were subjected to fluorescence and immunofluorescence microscopy, using polyclonal antiserum against human Pex14p (Will *et al*, 1999). The secondary antibodies used were anti-mouse IgGs, conjugated with Alexa Fluor-594 (Molecular Probes). All micrographs were recorded on a Zeiss Axioplan 2 microscope with a Zeiss Plan-Apochromat 63 × /1.4 oil objective and an Axiocam MR digital camera, and were processed with AxioVision 4.6 software (Zeiss, Jena, Germany). The steady-state level of Pex19p

expression was assessed by immunoblot analyses, using monoclonal mouse antibodies against *Hs*Pex19p (BD Biosciences).

Supplementary data
Supplementary data are available at *The EMBO Journal* Online (http://www.embojournal.org).

Acknowledgements

We thank Janica Meine for laboratory support and Marc Fransen (Katholieke Universiteit Leuven, Belgium) for fruitful discussions during the early phase of the project. Ron Wanders (AMC Amsterdam, The Netherlands) has kindly provided *PEX19*-deficient skin fibroblasts. Manfred Roessle is thanked for technical assistance to obtain SAXS data. Vivian Pogenberg is thanked for critical assessment and advice on fluorescence-polarization experiments. Chris Williams (EMBL) is thanked for critical comments on the experimental approach and the paper. The project has been supported by 3D-REPERTOIRE (EC, LSHG-CT-2005512028) to MW.

Author contributions: NS and SJH designed and carried out most of the experiments and contributed to writing of the paper. KF, MM, WAS, YHS, JW and WS carried out specific experiments and wrote the respective experiment sections in the paper. RE supported the work by JW and WS. MW coordinated the project and wrote the paper.

Conflict of interest

The authors declare that they have no conflict of interest.

References

Eckert JH, Erdmann R (2003) Peroxisome biogenesis. *Rev Physiol Biochem Pharmacol* **147:** 75–121

Emsley P, Cowtan K (2004) Coot: model-building tools for molecular graphics. *Acta Crystallogr D Biol Crystallogr* **60** (Part 12 Part 1)**:** 2126–2132

Fang Y, Morrell JC, Jones JM, Gould SJ (2004) PEX3 functions as a PEX19 docking factor in the import of class I peroxisomal membrane proteins. *J Cell Biol* **164:** 863–875

Fransen M, Brees C, Ghys K, Amery L, Mannaerts GP, Ladant D, Van Veldhoven PP (2002) Analysis of mammalian peroxin interactions using a non-transcription-based bacterial two-hybrid assay. *Mol Cell Proteomics* **1:** 243–252

Fransen M, Vastiau I, Brees C, Brys V, Mannaerts GP, Van Veldhoven PP (2004) Potential role for Pex19p in assembly of PTS-receptor docking complexes. *J Biol Chem* **279:** 12615–12624

Fransen M, Vastiau I, Brees C, Brys V, Mannaerts GP, Van Veldhoven PP (2005) Analysis of human Pex19p's domain structure by pentapeptide scanning mutagenesis. *J Mol Biol* **346:** 1275–1286

Fransen M, Wylin T, Brees C, Mannaerts GP, Van Veldhoven PP (2001) Human pex19p binds peroxisomal integral membrane proteins at regions distinct from their sorting sequences. *Mol Cell Biol* **21:** 4413–4424

Gatto Jr GJ, Geisbrecht BV, Gould SJ, Berg JM (2000) Peroxisomal targeting signal-1 recognition by the TPR domains of human PEX5. *Nat Struct Biol* **7:** 1091–1095

Gotte K, Girzalsky W, Linkert M, Baumgart E, Kammerer S, Kunau WH, Erdmann R (1998) Pex19p, a farnesylated protein essential for peroxisome biogenesis. *Mol Cell Biol* **18:** 616–628

Halbach A, Landgraf C, Lorenzen S, Rosenkranz K, Volkmer-Engert R, Erdmann R, Rottensteiner H (2006) Targeting of the tail-anchored peroxisomal membrane proteins PEX26 and PEX15 occurs through C-terminal PEX19-binding sites. *J Cell Sci* **119** (Part 12)**:** 2508–2517

Halbach A, Lorenzen S, Landgraf C, Volkmer-Engert R, Erdmann R, Rottensteiner H (2005) Function of the PEX19-binding site of human adrenoleukodystrophy protein as targeting motif in man and yeast. PMP targeting is evolutionarily conserved. *J Biol Chem* **280:** 21176–21182

Heiland I, Erdmann R (2005) Biogenesis of peroxisomes. Topogenesis of the peroxisomal membrane and matrix proteins. *FEBS J* **272:** 2362–2372

Hoepfner D, Schildknegt D, Braakman I, Philippsen P, Tabak HF (2005) Contribution of the endoplasmic reticulum to peroxisome formation. *Cell* **122:** 85–95

Jones JM, Morrell JC, Gould SJ (2001) Multiple distinct targeting signals in integral peroxisomal membrane proteins. *J Cell Biol* **153:** 1141–1150

Jones JM, Morrell JC, Gould SJ (2004) PEX19 is a predominantly cytosolic chaperone and import receptor for class 1 peroxisomal membrane proteins. *J Cell Biol* **164:** 57–67

Kammerer S, Arnold N, Gutensohn W, Mewes HW, Kunau WH, Hofler G, Roscher AA, Braun A (1997) Genomic organization and molecular characterization of a gene encoding HsPXF, a human peroxisomal farnesylated protein. *Genomics* **45:** 200–210

Matsuzaki T, Fujiki Y (2008) The peroxisomal membrane protein import receptor Pex3p is directly transported to peroxisomes by a novel Pex19p- and Pex16p-dependent pathway. *J Cell Biol* **183:** 1275–1286

Matsuzono Y, Kinoshita N, Tamura S, Shimozawa N, Hamasaki M, Ghaedi K, Wanders RJ, Suzuki Y, Kondo N, Fujiki Y (1999) Human PEX19: cDNA cloning by functional complementation, mutation analysis in a patient with Zellweger syndrome, and potential role in peroxisomal membrane assembly. *Proc Natl Acad Sci USA* **96:** 2116–2121

Matsuzono Y, Matsuzaki T, Fujiki Y (2006) Functional domain mapping of peroxin Pex19p: interaction with Pex3p is essential for function and translocation. *J Cell Sci* **119** (Part 17)**:** 3539–3550

Mayerhofer PU, Kattenfeld T, Roscher AA, Muntau AC (2002) Two splice variants of human PEX19 exhibit distinct functions in peroxisomal assembly. *Biochem Biophys Res Commun* **291:** 1180–1186

Mueller-Dieckmann J (2006) The open-access high-throughput crystallization facility at EMBL Hamburg. *Acta Crystallogr D Biol Crystallogr* **62** (Part 12)**:** 1446–1452

Muntau AC, Roscher AA, Kunau WH, Dodt G (2003) Interaction of PEX3 and PEX19 visualized by fluorescence resonance energy transfer (FRET). *Adv Exp Med Biol* **544:** 221–224

Neufeld C, Filipp FV, Simon B, Neuhaus A, Schuller N, David C, Kooshapur H, Madl T, Erdmann R, Schliebs W, Wilmanns M, Sattler M (2009) Structural basis for competitive interactions of Pex14 with the import receptors Pex5 and Pex19. *EMBO J* **28:** 745–754

Pape T, Schneider TR (2004) HKL2MAP: a graphical user interface for phasing with SHELX programs. *J Appl Cryst* **37:** 843–844

Pearson WR (1994) Using the FASTA program to search protein and DNA sequence databases. *Methods Mol Biol* **24:** 307–331

Pinto MP, Grou CP, Alencastre IS, Oliveira ME, Sa-Miranda C, Fransen M, Azevedo JE (2006) The import competence of a peroxisomal membrane protein is determined by Pex19p before the docking step. *J Biol Chem* **281:** 34492–34502

Pogenberg V, Guichou JF, Vivat-Hannah V, Kammerer S, Pérez E, Germain P, de Lera AR, Gronemeyer H, Royer CA, Bourguet W (2005) Characterization of the interaction between retinoic acid receptor/retinoid X receptor (RAR/RXR) heterodimers and transcriptional coactivators through structural and fluorescence anisotropy studies. *J Biol Chem* **280:** 1625–1633

Project CC (1994) The CCP4 suite: programs for protein crystallography. *Acta Cryst D* **50:** 760–763

Rottensteiner H, Kramer A, Lorenzen S, Stein K, Landgraf C, Volkmer-Engert R, Erdmann R (2004) Peroxisomal membrane proteins contain common Pex19p-binding sites that are an integral part of their targeting signals. *Mol Biol Cell* **15:** 3406–3417

Rucktaschel R, Thoms S, Sidorovitch V, Halbach A, Pechlivanis M, Volkmer-Engert R, Alexandrov K, Kuhlmann J, Rottensteiner H, Erdmann R (2009) Farnesylation of Pex19p is required for its structural integrity and function in peroxisome biogenesis. *J Biol Chem* **284:** 20885–20896

Schliebs W, Kunau WH (2006) PTS2 co-receptors: diverse proteins with common features. *Biochim Biophys Acta* **1763:** 1605–1612

Shibata H, Kashiwayama Y, Imanaka T, Kato H (2004) Domain architecture and activity of human Pex19p, a chaperone-like protein for intracellular trafficking of peroxisomal membrane proteins. *J Biol Chem* **279:** 38486–38494

Stanley WA, Filipp FV, Kursula P, Schuller N, Erdmann R, Schliebs W, Sattler M, Wilmanns M (2006) Recognition of a functional peroxisome type 1 target by the dynamic import receptor pex5p. *Mol Cell* **24:** 653–663

Stanley WA, Fodor K, Marti-Renom MA, Schliebs W, Wilmanns M (2007a) Protein translocation into peroxisomes by ring-shaped import receptors. *FEBS Lett* **581:** 4795–4802

Stanley WA, Pursiainen NV, Garman EF, Juffer AH, Wilmanns M, Kursula P (2007b) A previously unobserved conformation for the human Pex5p receptor suggests roles for intrinsic flexibility and rigid domain motions in ligand binding. *BMC Struct Biol* **7:** 24

Terwilliger TC (2003) Automated main-chain model building by template matching and iterative fragment extension. *Acta Crystallogr D Biol Crystallogr* **59** (Part 1)**:** 38–44

Vastiau IM, Anthonio EA, Brams M, Brees C, Young SG, Van de Velde S, Wanders RJ, Mannaerts GP, Baes M, Van Veldhoven PP, Fransen M (2006) Farnesylation of Pex19p is not essential for peroxisome biogenesis in yeast and mammalian cells. *Cell Mol Life Sci* **63:** 1686–1699

Vizeacoumar FJ, Vreden WN, Aitchison JD, Rachubinski RA (2006) Pex19p binds Pex30p and Pex32p at regions required for their peroxisomal localization but separate from their peroxisomal targeting signals. *J Biol Chem* **281:** 14805–14812

Will GK, Soukupova M, Hong X, Erdmann KS, Kiel JA, Dodt G, Kunau WH, Erdmann R (1999) Identification and characterization of the human orthologue of yeast Pex14p. *Mol Cell Biol* **19:** 2265–2277

